Skewed Slab-on-Girder Steel Bridge Superstructures with Bidirectional-Ductile End Diaphragms

Oguz C. Celik, A.M.ASCE[1]; and Michel Bruneau, F.ASCE[2]

Abstract: Specially designed ductile end diaphragms of steel bridge superstructures have previously proved, both theoretically and experimentally, to dissipate seismic input energy, protecting other substructure and superstructure members. Although ductile diaphragms have been introduced in the latest AASHTO guide specifications as a structural system that can be used to resist transverse earthquake effects, no guidance is provided on how to implement these ductile diaphragms in skewed bridges. To address this need and to resolve some shortcomings of the known end diaphragm systems (EDSs), two bidirectional end diaphragm configurations, namely, EDS-1 and EDS-2, with buckling restrained braces (BRBs) are proposed and numerically investigated. Bidirectional end diaphragm is a new concept, and can be implemented both in straight and skewed steel bridge superstructures to resist bidirectional earthquake effects. To assess the relative effectiveness of the proposed systems and to investigate how various parameters relate to seismic response, closed-form solutions are developed using nondimensional bridge geometric ratios. Numerical results indicate that skewness more severely affects end diaphragm behavior when $\varphi \geq 30°$. Also, comparisons reveal that although both end diaphragm systems can be used with confidence as ductile seismic fuses, each of the two systems considered have advantages that may favor its implementation, depending on project-specific constraints. **DOI: 10.1061/(ASCE)BE.1943-5592.0000141.** © 2011 American Society of Civil Engineers.

CE Database subject headings: Bridges, skew; Bridges, steel; Buckling; Bracing; Energy dissipation; Ductility; Diaphragms; Earthquakes.

Author keywords: Skewed steel bridges; Seismic retrofit; Buckling restrained braces (BRBs); Hysteretic energy dissipation; Ductile end diaphragms; Bidirectional earthquake effects.

Introduction

The recently published *AASHTO Seismic Guide Specifications for LRFD Seismic Bridge Design* include provisions for the design of steel bridges having specially detailed ductile diaphragms to resist loads applied in the bridge transverse direction (AASHTO 2009; closely following the recommendations in MCEER/ATC 2003). Previous studies (e.g., Zahrai and Bruneau 1999a, b; Carden et al. 2006) support that significant energy can be dissipated in ductile bridge-end diaphragms, while reducing seismic demands in other substructure and superstructure elements. Past research has shown how shear panel systems (SPSs), steel triangular plate added damping and stiffness devices (TADAs), eccentrically braced end diaphragms (EBFs), and buckling restrained braces (BRBs—also called unbonded braces) could be detailed to provide an appropriate seismic performance. Ductile performance requires special detailing such as that evinced by bridge-end diaphragm damage in prior earthquakes (Bruneau et al. 1996; Itani et al. 2004).

Currently, ductile diaphragms have to be combined with other lateral load resisting strategies to address seismic excitations along the bridge's longitudinal axis. Also, AASHTO (2009) provides no guidance on how to implement ductile diaphragms in skewed bridges—even though steel bridges with skewed superstructure geometries are commonly encountered at highway interchanges, river crossings, and other places because of alignment limitations.

This paper investigates the seismic response of the proposed concept to implement ductile end diaphragms in skewed bridge superstructures, at the same time resisting bidirectional earthquake excitations—implementation in nonskewed straight bridges being a special case of the general formulation. Here, BRBs are used as the diaphragm ductile seismic fuses. BRBs have been implemented in many buildings in Japan and in the United States on account of their stable unpinched hysteretic characteristics, ease of design, and ability to eliminate seismically induced structural damage and provide satisfactory seismic performance. BRBs have also been used to retrofit the Minato Bridge in Japan (Kanaji et al. 2003), the world's third-longest truss bridge, using a concept similar to the ductile cross-frame system developed by Sarraf and Bruneau (1998a, b) and analogous to the ductile diaphragm concept.

Here, two proposed end diaphragm systems (EDSs) (i.e., geometrical layouts) are considered, namely, EDS-1 and EDS-2. Although they are considered here in the perspective of new bridge design, the information presented is also applicable to existing bridges for seismic retrofit purposes. Results from parametric studies are used to formulate design recommendations.

[1]Professor, Div. of Theory of Structures, Faculty of Architecture, Istanbul Technical Univ., Taskisla, Taksim, Istanbul 34437, Turkey; formerly, Research Scientist, Dept. of CSEE, Univ. at Buffalo, Amherst, NY 14260. E-mail: celikoguz@itu.edu.tr

[2]Professor, Dept. of CSEE, Univ. at Buffalo, Amherst, NY 14260. E-mail: bruneau@buffalo.edu

Proposed Ductile End Diaphragm Configurations with BRBs

This study focuses on two types of ductile bracing configurations in bridge-end diaphragms:

- *EDS-1:* Two pairs of BRBs are installed at each end of a span, in a configuration that coincides with the skew and longitudinal directions [Fig. 1(a)].
- *EDS-2:* A single pair of BRBs is installed at each end of a span, at an angle that does not coincide with the bridge longitudinal and skew directions [Fig. 1(b)].

In EDS-1, the bottom connection of the pair of BRBs oriented in the skew direction can be connected either to the abutment or between web stiffeners of the bridge girders. The latter choice is common for steel bridges. The pair of longitudinal BRBs is a new concept and needs to be connected either to the horizontal, next to the bearings, or to the vertical face of the abutments—as would be the BRBs in EDS-2. The BRBs connecting to the abutment need to be in series with lock-up devices that allow thermal expansion under normal conditions but engage the BRBs during earthquakes. For the deck-level connection, specially designed cross beams are required to elastically resist forces from the BRBs, unless connection to the existing interior cross-frames or girders is developed without damaging any internal component (capacity design).

Since significant forces may develop in the BRBs, all components to which the BRBs connect should be checked to ensure that they are able to resist such forces without yielding and without undesirable deformations. Some details developed by other researchers to connect ductile diaphragms to bridge decks can be useful for this purpose (Carden et al. 2006). Details that do not induce

large moments at the BRB's ends may be also desirable. Examples of such BRB connections are available in Lopez and Sabelli (2004).

Modeling Assumptions

Neoprene bearings, bidirectional sliding bearings, and other bearings with negligible strength to horizontal deformations—and to some degree even bearings damaged by an earthquake that could still slide in a stable manner—are considered here. This case is called the *floating span*. Floating span–type bridges have no resistance to lateral earthquake loading and therefore need to be restrained laterally by ductile seismic devices, shear keys, or elastic end diaphragms to limit their horizontal displacements. In this study, the BRBs serve as an alternative and seismically effective choice.

To check numerical results obtained from computer analysis using simple models, closed-form solutions are also presented. To help reduce the complexity of the derived expressions, an ideal elastic-plastic hysteretic model with equal tension and compression capacities $T_y = C_y$ is used for the BRBs (Black et al. 2002; Sabelli et al. 2003; Celik and Bruneau 2007). Furthermore, the BRBs are assumed to have pinned end connections and are not active under gravity loading. Cross-sectional areas of BRBs and skew angles are taken to be the same for each of the two end diaphragms used in each specific bridge. Furthermore, the rigid concrete deck and the steel girders are continuously connected, i.e., composite girders, but are assumed to be fully flexible about their connection axis, parallel to the bridge axis. The angle between the plane of the concrete deck and the plane of the steel beam can change without developing out-of-plane flexural moments.

Zahrai and Bruneau (1998) demonstrated that seismic demand under lateral load concentrates at the end diaphragms of steel slab-on-girder bridge superstructures and that the presence of intermediate cross braces does not affect the seismic behavior of these bridges and can be neglected. This demonstration leads to a simplified structural model to simulate the system behavior. Results from the nonlinear finite-element analyses by Zahrai and Bruneau (1998), which considered the complete bridge system—that is the concrete deck, steel girders, and all diaphragms, provide substantial confidence in the ability of the simplified model to capture all the key aspects of bridge response of interest here. For EDS-2, the steps followed to idealize a typical bridge with end diaphragms into a simpler model are given in Fig. 2. Further details and a similar process of idealization followed for EDS-1 are given in Celik and Bruneau (2007). These analytical models account for general system geometric dimensions such as the skew angle (φ), girder spacing (s), end diaphragm depth (d), and length to internal diaphragm anchor point (a), as well as bidirectional earthquake effects. Results from this study can help select an appropriate value for the parameter a.
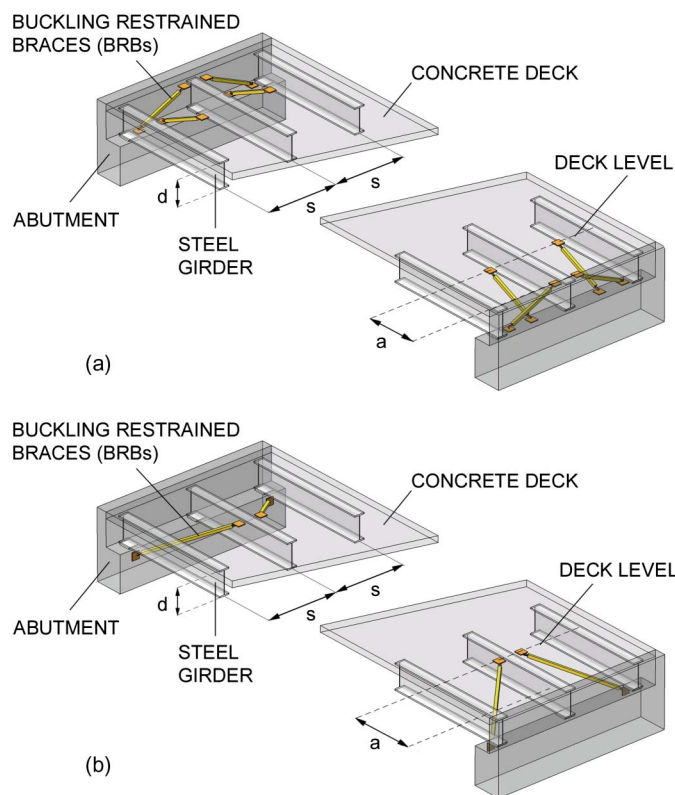
End Diaphragm System-1

Analytical results of interest include base shear forces at yield; yield displacements or drifts; member versus global (system) ductility relationships; initial stiffness of the end diaphragm system, which is needed for response spectrum analysis; and total or volumetric hysteretic energy dissipations, in both orthogonal bridge directions as applicable. Results from this investigation can be used to assess the effectiveness of various configurations of ductile diaphragms in skewed bridges. Static pushover analyses are also carried out on a set of selected end diaphragm configurations using SAP2000 (CSI 1998) to validate the analytical equations formulated, and to aid in understanding the impact of several
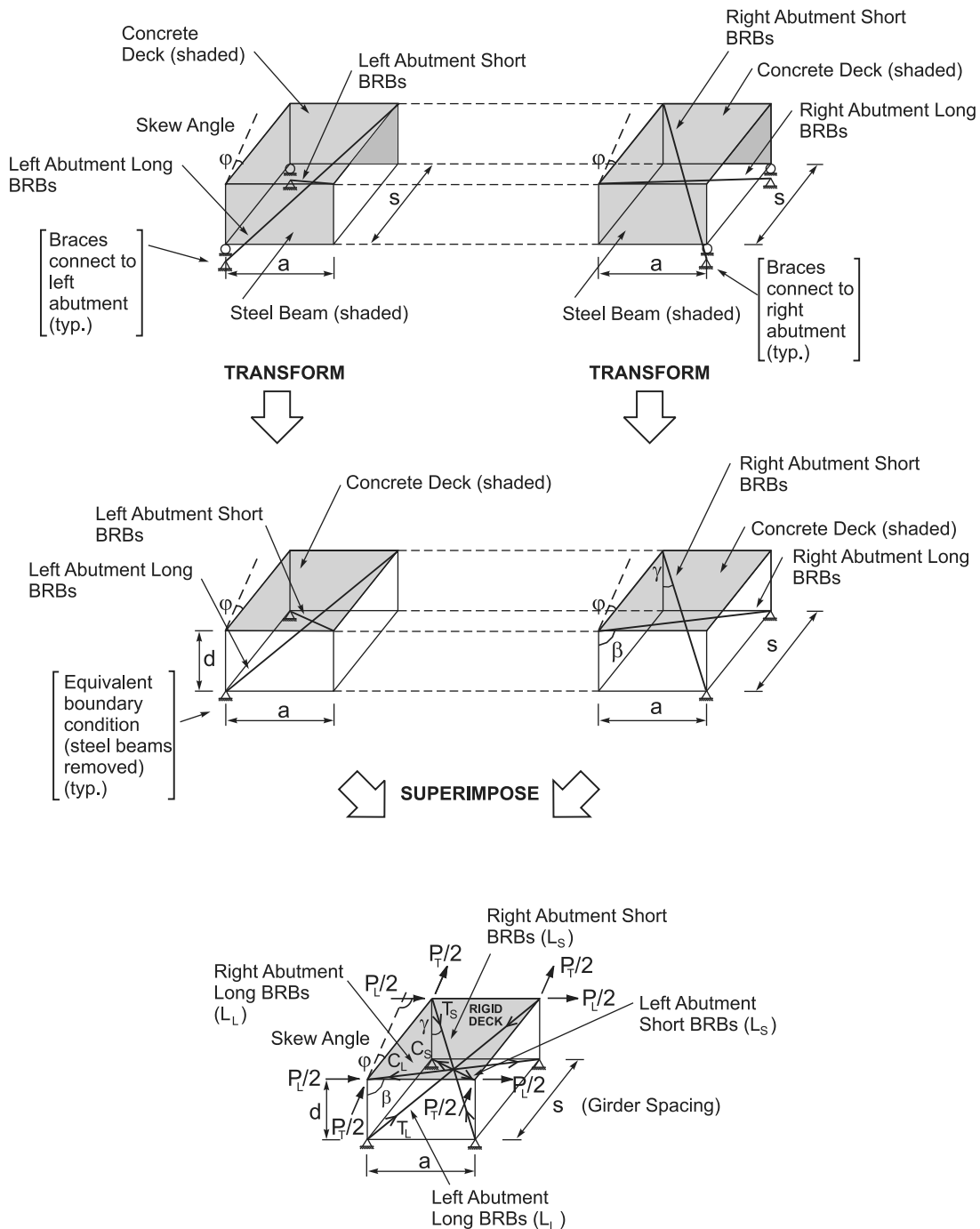

Fig. 1. Proposed end diaphragm systems (EDSs) for steel bridges: (a) EDS-1; (b) EDS-2 (intermediate cross-frames not shown for clarity)

Fig. 2. System idealization steps for EDS-2

system parameters on the inelastic response of bridges with bidirectionally acting end diaphragms.

Nonlinear pushover analysis is adopted in this paper. Equal proportions of the total lateral load in a given direction are applied at each corner of the deck. P_L and P_T are the lateral earthquake loads acting at the deck level on one diaphragm in the longitudinal and transverse directions, respectively. The bidirectional loading ratio of P_L/P_T or P_T/P_L is typically set constant in the pushover analyses. As the system yields in one direction, the forces cannot increase anymore, and the displacement path "bifurcates" toward the yielding direction. Pushover stops when the prescribed axial displacement ductility level (i.e., μ) of the BRBs is reached.

Dissipated energy is calculated when the arbitrarily selected BRB ductility limit is reached.

Previous studies (e.g., Black et al. 2002) showed that the ductility capacities of BRBs, here called, "member ductility" and considered to be a local ductility, are typically greater than $\mu = 20$, which typically corresponds to a drift ratio of 2–3%. Here, an average value of $\mu = 10$ is considered as a target-member ductility in developing diagrams. Global ductility is related to local member ductility per the equations that this paper presents. Higher ductility demands correspond to larger drifts; the engineer must ensure that such drifts will not damage other substructure and superstructure elements.

Elastic Behavior and BRBs Axial Force Ratio

With reference to the three-dimensional idealized truss system given in Fig. 3, total longitudinal and transverse direction base shear forces in the elastic range are equal to $V_L = 2P_L$ and $V_T = 2P_T$, respectively, since two end diaphragms are considered in this model. Static equilibrium gives the following BRB axial force ratio under bidirectional loading:

$$\frac{C_L}{C_S} = \frac{T_L}{T_S} = \sqrt{\frac{1 + (d/a)^2}{1 + (d/s)^2}}(P_L/P_T \cos \varphi - \sin \varphi) \qquad (1)$$

where T_L, C_L, T_S, and C_S show tension and compression forces in the longitudinal (L) and skew (S) BRBs, respectively. Depending on the axial force ratios, the possible limit states for this system are as follows:

- If $C_L/C_S = T_L/T_S < 1$, then the BRBs in the skew direction yield first;
- If $C_L/C_S = T_L/T_S > 1$, then the longitudinal BRBs yield first;
- If $C_L/C_S = T_L/T_S = 1$, then all the BRBs yield at the same time.

On the basis of a survey of bridge inventories in North America, it was decided to consider numerical values of d/s of 0.25, 0.50, 1.00, 1.25, and 1.50, a range covering most short and medium span slab-on-girder and deck-truss steel bridges, as well as values of d/a equal to 0.20, 0.40, 0.60, 0.80, and 1.00 (Celik and Bruneau 2007). Since many bridge standards and regulations rely on one of two simplified combination rules to account for bidirectional earthquake effects, here both the 30% rule (AASHTO 2002) and the 40% rule (ATC-32 1996) were considered to show the impact of this value on the BRBs' axial force ratio.

For a given end diaphragm variable's value, for example, $d/s = 0.40$, as an average value for many slab-on-girder bridges in North America, the variation of force ratio with respect to the skew angle can be investigated for different values of d/a and P_L/P_T, or P_T/P_L. For $P_L/P_T = 0.30$ and 0.40, for example, Fig. 4 shows that the absolute value of the axial force ratio increases as the skew angle increases. For relatively small skew angles, say, $\varphi \leq 30°$, changes in the d/a ratio have no significant effect on the ratio of elastic forces in the longitudinal and transverse BRBs. For $P_T/P_L = 0.30$ and 0.40, the axial force ratio decreases as the skew angle increases. Changes in the d/a ratio are more visible at smaller skew angles for $P_T/P_L = 0.30$ and 0.40.
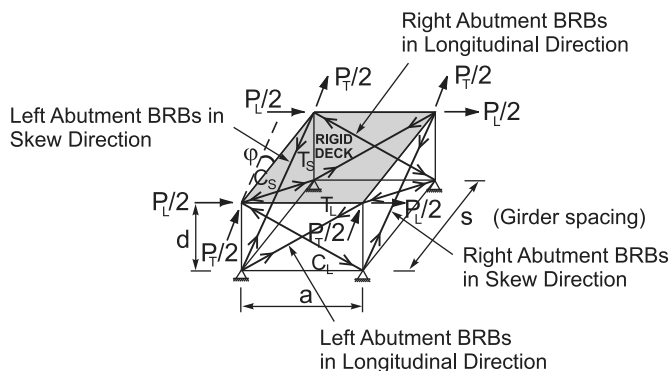

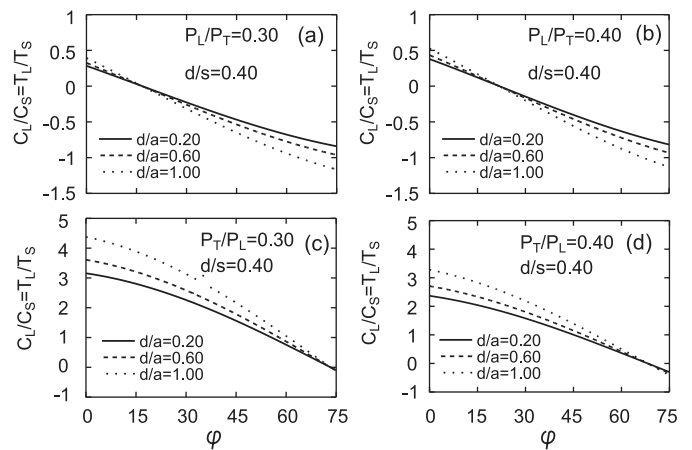**Fig. 3.** Bidirectional loading and BRB forces for EDS-1

Fig. 4. Variation of BRB elastic axial forces ratio with bridge geometric relations and skew angle (φ) (for EDS-1 and $d/s = 0.40$): (a) for $P_L/P_T = 0.30$; (b) for $P_L/P_T = 0.40$; (c) for $P_T/P_L = 0.30$; (d) for $P_T/P_L = 0.40$

Inelastic Behavior When Skew BRBs Yield

Since bridge response is bidirectional because of both bidirectional loading and the skew angle, transverse and longitudinal responses are investigated separately for each yielding mechanism.

Response in the Transverse Direction

Fig. 5 shows the typical hysteretic curve of the system in both the transverse and longitudinal directions. When $C_S, T_S > C_L, T_L$, the skew braces yield only, and base shear strength (V_{yT}), yield displacement (Δ_{yT}) and corresponding drift (Δ_{yT}/d) at yield, global ductility (μ_{GT}), and the stiffness of the system (K_T) in the transverse direction can be obtained depending on the bridge geometry and BRB properties as follows:

Using equilibrium in the transverse direction, the base shear component in the transverse direction (V_{yT}) can be calculated by substituting C_y, T_y, the axial yield strength of BRBs, F_yA for C_S and T_S, axial forces in the skew yielding braces:

$$V_{yT} = \frac{n_S \cos \varphi}{\sqrt{1 + (d/s)^2}}(F_yA) \qquad (2)$$

where F_y and A are the yield stress and the cross-sectional area of each brace. Note that only the skew BRBs contribute to base shear strength in the transverse direction. As subsequently shown, n_S and n_L, are the number of BRBs placed in the skew and longitudinal directions, respectively. Equal numbers of BRBs in both directions are used in this study, i.e,. $n = n_S = n_L$.

Lateral displacements of the system can be determined using the method of virtual work. According to this analysis procedure, an external virtual unit load is applied in the direction of unknown top displacement. Virtual axial forces are then calculated in the BRBs. Equating the work of external loads and the work of internal forces gives the desired displacement. Further details can be found in Celik and Bruneau (2007). Following this procedure gives the lateral displacement in the transverse direction as

$$\Delta_T = \frac{L_S^3 a^2 \mu - L_L^3 s^2 \sin \varphi (P_L/P_T \cos \varphi - \sin \varphi)}{L_S a^2 s \cos \varphi}\left(\frac{F_y}{E}\right) \qquad (3)$$

where μ is the displacement ductility for a single BRB used, E is the modulus of elasticity of steel, and L_S and L_L are the lengths of the BRBs in the skew and longitudinal directions, respectively. Knowing the yield displacement also allows us to evaluate the initial stiffness as well as the fundamental period for response in both orthogonal directions. Rewriting Eq. (3) using nondimensional bridge geometrical properties and substituting $\mu = 1$ give the transverse drift (i.e., Δ_{yT}/d) at yielding of the skew BRBs as follows:

$$\frac{\Delta_{yT}}{d} = \frac{[1 + (d/s)^2]^{3/2}(d/a) - [1 + (d/a)^2]^{3/2}(d/s)\sin\varphi(P_L/P_T\cos\varphi - \sin\varphi)}{(d/a)(d/s)\sqrt{1 + (d/s)^2}\cos\varphi}\left(\frac{F_y}{E}\right) \tag{4}$$

This equation accounts for the contributions of yielding and elastic, i.e., nonyielding, BRBs. The ratio of maximum displacement to the yield displacement in the transverse direction (i.e., the system global ductility, μ_{GT}) can be obtained by the ratio of the displacements that correspond to $\mu = \mu$ and $\mu = 1$. Hence,

$$\mu_{GT} = \frac{[1 + (d/s)^2]^{3/2}(d/a)\mu - [1 + (d/a)^2]^{3/2}(d/s)(P_L/P_T\cos\varphi - \sin\varphi)\sin\varphi}{[1 + (d/s)^2]^{3/2}(d/a) - [1 + (d/a)^2]^{3/2}(d/s)(P_L/P_T\cos\varphi - \sin\varphi)\sin\varphi} \tag{5}$$

Dividing Eq. (2) by Eq. (4) gives the initial stiffness (K_T) of the system in the transverse direction. This result leads to

$$K_T = \frac{n(d/s)(d/a)\cos^2\varphi}{[1 + (d/s)^2]^{3/2}(d/a) - [1 + (d/a)^2]^{3/2}(d/s)(P_L/P_T\cos\varphi - \sin\varphi)\sin\varphi}\left(\frac{EA}{d}\right) \tag{6}$$

which enables us to evaluate the initial stiffness of the system in terms of axial stiffness of the BRB.

Hysteretic energy dissipation (E_H) during a complete cycle is given by the shaded area in Fig. 5, or equivalently, the same hysteresis can be calculated from the sum of the hysteretic energy for all individual yielding members. Also, the corresponding hysteretic energy per total brace volume (Vol.) is useful for comparison purposes. Performing this calculation gives:

$$\frac{E_H}{\text{Vol.}} = \frac{4(\mu - 1)}{1 + \frac{(d/s)}{(d/a)}\sqrt{\frac{1 + (d/a)^2}{1 + (d/s)^2}}}\left(\frac{F_y^2}{E}\right) \tag{7}$$

Response in the Longitudinal Direction
In a similar manner, base shear, yield drift, and initial stiffness can be calculated for response in the longitudinal direction. The longitudinal component of base shear (V_L) when the skew BRBs yield is equal to the following:

$$V_L = \frac{n_S\sin\varphi + n_L(P_L/P_T\cos\varphi - \sin\varphi)}{\sqrt{1 + (d/s)^2}}(F_yA)$$
$$= \frac{nP_L/P_T\cos\varphi}{\sqrt{1 + (d/s)^2}}(F_yA) \tag{8}$$

Using the longitudinal displacement (Δ_L), drift at yielding of skew BRBs can be expressed as

$$\frac{\Delta_L}{d} = \frac{[1 + (d/a)^2]^{3/2}(P_L/P_T\cos\varphi - \sin\varphi)}{(d/a)\sqrt{1 + (d/s)^2}}\left(\frac{F_y}{E}\right) \tag{9}$$

Note that Eq. (9) does not include the member ductility term, revealing that there is no energy dissipation in the longitudinal direction BRBs. Therefore, during reversed cyclic loading, only elastic recovery takes place; and after yielding of the skew BRBs, displacement in the longitudinal direction remains unchanged while the displacement in the other direction increases.

Using Eqs. (8) and (9), initial stiffness in the longitudinal direction can be obtained as

$$K_L = \frac{n(d/a)P_L/P_T\cos\varphi}{[1 + (d/a)^2]^{3/2}(P_L/P_T\cos\varphi - \sin\varphi)}\left(\frac{EA}{d}\right) \tag{10}$$

Here, a 345 MPa (50 ksi) grade steel with $E = 200000$ MPa (29000 ksi) is assumed for the results presented. Fig. 6(a) shows the variation of nondimensional transverse base shear as a function of end diaphragm geometric ratios when skew BRBs yield. A decrease occurs in this value as the d/s ratio and skew angle (φ) increase because of larger direction angles resulting in smaller horizontal force components. For $d/s = 0.40$, transverse drift (Δ_{yT}/d) at yield versus φ is illustrated in Fig. 6(b) per Eq. (4), revealing that drift increases as φ increases. The rate of this increase is more at large skew angles when $\varphi \geq 30°$. Variation of nondimensional transverse stiffness is given in Fig. 6(c), showing a rapid
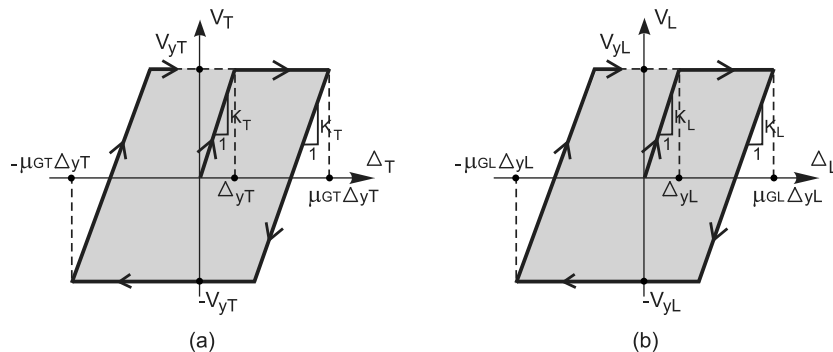

(a)

(b)

Fig. 5. Transverse and longitudinal base shear versus displacement hysteretic curves for proposed EDSs

decrease in stiffness at large skew angles (again when $\varphi \geq 30°$). While the impact of d/a ratio on drift is more pronounced at large skew angles, stiffness is less affected by this ratio at large skew angles since the variation of base shear is small. Global transverse ductility ratio is plotted against φ in Fig. 6(d). This ratio is more affected by the d/a ratio at large skew angles. Nondimensional base shear in the longitudinal direction versus φ is given in Fig. 6(e), showing a similar response to transverse behavior. Similar trends are observed for other behavioral parameters in the longitudinal direction, not presented here because of space constraints. For $\mu = 10$, Fig. 6(f) illustrates that nondimensional dissipated hysteretic energy increases as d/a increases for constant values of d/s, which could be important in an existing bridge retrofit design, but decreases as d/s increases for constant values of d/a, which could be important in a new bridge design. Smaller d/s ratios

corresponding to fewer girders, or girders with larger spacing, therefore result in more energy dissipation in the system.

Inelastic Behavior When Longitudinal BRBs Yield

Response in the Transverse Direction
Yielding BRBs do not contribute to base shear strength in the transverse direction, since they are in the other orthogonal direction. Therefore, only unyielding BRBs should be considered for the transverse base shear strength. This gives

$$V_T = \frac{n \cos \varphi}{\sqrt{1 + (d/a)^2}(P_L/P_T \cos \varphi - \sin \varphi)} (F_y A) \quad (11)$$

The transverse drift (taking $\mu = 1$) can be calculated as before. The resulting equation is

$$\frac{\Delta_T}{d} = \frac{-(d/s)[1 + (d/a)^2]^{3/2}(P_L/P_T \cos \varphi - \sin \varphi) \sin \varphi + (d/a)[1 + (d/s)^2]^{3/2}}{(d/a)(d/s)\sqrt{1 + (d/a)^2}(P_L/P_T \cos \varphi - \sin \varphi) \cos \varphi} \left(\frac{F_y}{E}\right) \quad (12)$$

Base shear strength given in Eq. (11) and the yield drift given in Eq. (12) are sufficient to obtain the hysteretic curve of the system, shown in Fig. 5. The global system ductility, μ_{GT}, can be calculated by the ratio of the maximum and yield displacements as

$$\mu_{GT} = \frac{-(d/s)[1 + (d/a)^2]^{3/2} \sin \varphi(P_L/P_T \cos \varphi - \sin \varphi)\mu + (d/a)[1 + (d/s)^2]^{3/2}}{-(d/s)[1 + (d/a)^2]^{3/2} \sin \varphi(P_L/P_T \cos \varphi - \sin \varphi) + (d/a)[1 + (d/s)^2]^{3/2}} \quad (13)$$

Also, the initial stiffness is found to be

$$K_T = \frac{n(d/a)(d/s)\cos^2\varphi}{-(d/s)[1 + (d/a)^2]^{3/2}(P_L/P_T \cos \varphi - \sin \varphi) \sin \varphi + (d/a)[1 + (d/s)^2]^{3/2}} \left(\frac{EA}{d}\right) \quad (14)$$

The dissipated energy per total BRB volume during a single full cycle can be written as

$$\frac{E_H}{\text{Vol.}} = \frac{4(\mu - 1)}{1 + \frac{(d/a)}{(d/s)}\sqrt{\frac{1+(d/s)^2}{1+(d/a)^2}}} \left(\frac{F_y^2}{E}\right) \quad (15)$$

Response in the Longitudinal Direction
Base shear in the longitudinal direction can be derived as

$$V_{yL} = \frac{n(P_L/P_T) \cos \varphi}{\sqrt{1 + (d/a)^2}(P_L/P_T \cos \varphi - \sin \varphi)} (F_y A) \quad (16)$$

The longitudinal yield drift in terms of nondimensional system geometric properties becomes

$$\frac{\Delta_{yL}}{d} = \frac{[1 + (d/a)^2]}{(d/a)} \left(\frac{F_y}{E}\right) \quad (17)$$

Skew BRBs do not contribute to the drift in the longitudinal direction. In this case, the global displacement ductility is equal to the member ductility:

$$\mu_{GL} = \frac{\Delta_L}{\Delta_{yL}} = \mu \quad (18)$$

Using Eqs. (16) and (17) gives the initial stiffness of the system in the longitudinal direction as

$$K_L = \frac{n(d/a)P_L/P_T \cos \varphi}{[1 + (d/a)^2]^{3/2}(P_L/P_T \cos \varphi - \sin \varphi)} \left(\frac{EA}{d}\right) \quad (19)$$

As shown in Eqs. (11)–(19), similar behavior trends are obtained for both transverse and longitudinal directions when

longitudinal BRBs yield, and diagrams similar to those presented in the previous section could be derived. From Eqs. (17) and (18), the longitudinal yield drift (Δ_{yL}/d) is independent of the skew angle (φ) and the global longitudinal ductility ratio is equal to the member (BRB) ductility.

EDS-2

Similar analytical expressions can be developed to describe the behavior of skewed bridges having the EDS-2 configuration of end diaphragms. Special cases are also considered to investigate the effect of certain parameters on the bidirectional seismic response of these bridges. Figs. 1(b) and 2 show the selected configuration of BRBs for EDS-2. In this case, BRB lengths differ from each other. The lengths of long (L_L) and short (L_S) BRBs can be given as

$$L_L = \sqrt{a^2 + s^2 + d^2 + 2as \sin \varphi} \quad (20)$$

$$L_S = \sqrt{a^2 + s^2 + d^2 - 2as \sin \varphi} \quad (21)$$

Elastic Behavior and BRBs Axial Force Ratio

For the system considered, it is convenient to evaluate the ratio of the elastic forces of short and long BRBs, to obtain load-displacement diagrams. Using the geometry in Fig. 2, elastic axial force ratio of the BRBs is obtained as follows

$$\frac{C_L}{C_S} = \frac{T_L}{T_S} = \sqrt{\frac{1 + (s/a)^2 + (d/a)^2 + 2(s/a)\sin\varphi}{1 + (s/a)^2 + (d/a)^2 - 2(s/a)\sin\varphi}}$$

$$\times \left[\frac{(s/a)(\sin\varphi - P_L/P_T\cos\varphi) - 1}{(s/a)(-\sin\varphi + P_L/P_T\cos\varphi) - 1}\right] \quad (22)$$

Here, C_S, T_S and C_L, T_L denote axial compression and tension forces in the short and longitudinal BRBs, respectively. In the elastic range, shear forces in each longitudinal and transverse direction are $V_L = 2P_L$ and $V_T = 2P_T$. The following are the possible limits of the brace force ratio and the corresponding meaning.

- If $C_L/C_S = T_L/T_S < 1$, then the short BRBs yield first;
- If $C_L/C_S = T_L/T_S > 1$, then the long BRBs yield first;
- If $C_L/C_S = T_L/T_S = 1$, then all BRBs yield at the same time.

For EDS-2, Fig. 7 shows the variation of the BRB axial forces ratio as a function of bridge geometry and the skew angle (φ). For $s/a = 0.50$, changes in the axial force ratio are depicted in Figs. 7(a) and 7(b) for $P_L/P_T = 0.30$ and 0.40, respectively. To show the impact of the s/a ratio on the axial force ratio,

taking $s/a = 1.00$ as constant and d/a as variable, Figs. 7(c) and 7(d) are plotted against φ for $P_L/P_T = 0.30$ and 0.40, respectively. In all cases, a decrease in the axial force ratio is observed as φ increases. Compared with the $s/a = 0.50$ case, changes in the axial force ratio are more pronounced in $s/a = 1.00$. Also, higher values are obtained for $s/a = 1.00$ and $P_L/P_T = 0.40$. The effect of d/a ratio on the axial force ratio increases as φ increases. For constant values of φ, the axial force ratio decreases as the d/a ratio increases.

Inelastic Behavior When Short BRBs Yield

Response in the Transverse Direction

To obtain the yield shear force in the transverse direction when short BRBs yield, the procedure followed for EDS-1 is repeated. The elastic brace forces are first replaced with the axial yield forces in the yielding BRBs. The other longer BRBs remain elastic up to the specified limit state. Writing the equations of equilibrium in the transverse direction gives the yield base shear in this direction as follows:

$$V_{yT} = \left[\frac{4(s/a)\cos\varphi}{\sqrt{1 + (s/a)^2 + (d/a)^2 - 2(s/a)\sin\varphi}[(s/a)(\sin\varphi - P_L/P_T\cos\varphi) + 1]}\right](F_yA) \quad (23)$$

Similarly, the yield drift in the transverse direction can be obtained as

$$\frac{\Delta_{yT}}{d} = \{[1 + (s/a)^2 + (d/a)^2 - 2(s/a)\sin\varphi]^{3/2}[(s/a)\sin\varphi + 1][(s/a)(P_L/P_T\cos\varphi - \sin\varphi) - 1]$$

$$+ [1 + (s/a)^2 + (d/a)^2 + 2(s/a)\sin\varphi]^{3/2}[(s/a)(P_L/P_T\cos\varphi - \sin\varphi) + 1][(s/a)\sin\varphi - 1]\}$$

$$\times \left(\frac{F_y}{E}\right)/2(d/a)(s/a)\sqrt{1 + (s/a)^2 + (d/a)^2 - 2(s/a)\sin\varphi}\cos\varphi[(s/a)(P_L/P_T\cos\varphi - \sin\varphi) - 1] \quad (24)$$

Response in the Longitudinal Direction

The following behavioral characteristics are reached for response in the longitudinal direction. The base shear in the longitudinal direction is found to be

$$V_{yL} = \left[\frac{4(s/a)P_L/P_T\cos\varphi}{\sqrt{1 + (s/a)^2 + (d/a)^2 - 2(s/a)\sin\varphi}[(s/a)(P_L/P_T\cos\varphi - \sin\varphi) - 1]}\right](F_yA) \quad (25)$$

And the corresponding drift in the longitudinal direction can be expressed as

$$\frac{\Delta_{yL}}{d} = \{[1 + (s/a)^2 + (d/a)^2 - 2(s/a)\sin\varphi]^{3/2}[(s/a)(\sin\varphi - P_L/P_T\cos\varphi) + 1]$$

$$+ [1 + (s/a)^2 + (d/a)^2 + 2(s/a)\sin\varphi]^{3/2}[(s/a)(\sin\varphi - P_L/P_T\cos\varphi) - 1]\}$$

$$\times \left(\frac{F_y}{E}\right)/2(d/a)\sqrt{1 + (s/a)^2 + (d/a)^2 - 2(s/a)\sin\varphi}[(s/a)(P_L/P_T\cos\varphi - \sin\varphi) - 1] \quad (26)$$

As before, the initial stiffness of the system in the transverse and longitudinal directions can be obtained from Eqs. (23)–(26). Since the resulting equations are too long, only numerical results are shown in Fig. 8.

Taking $d/a = 0.60$ as constant and s/a as variable, Fig. 8(a) shows the nondimensional transverse base shear strength as a function of the skew angle (φ). For constant values of s/a, a decrease in the nondimensional base shear is observed as φ increases. The s/a ratio has an important impact on the base shear at smaller skew angles. For constant values of φ, the base shear strength decreases

as s/a decreases, i.e., smaller base shears are obtained at smaller β angles. As shown in Fig. 8(b), the transverse yield drift (Δ_{yT}/d) increases as φ increases but decreases as s/a increases, revealing that BRBs with larger direction angles would be preferable to obtain stiffer end diaphragms. This also suggests that EDS-2 is more effective when sufficient girder spacing exists in the bridge superstructure. As expected, the increase in drift is less at smaller skew angles when $\varphi \le 30°$, suggesting that severely skewed systems should be avoided if possible. From Fig 8(c), the nondimensional transverse stiffness is observed to decrease as φ increases for
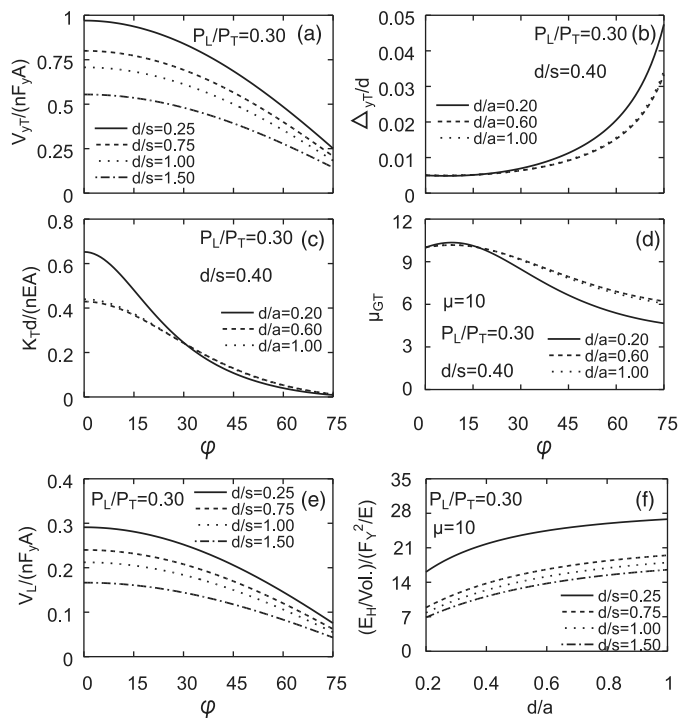
Fig. 6. Variation of behavioral characteristics when skew BRBs yield: (a) nondimensional transverse base shear strength versus skew angle (φ); (b) transverse yield drift versus φ; (c) nondimensional transverse stiffness versus φ; (d) global transverse ductility ratio versus φ; (e) nondimensional longitudinal base shear versus φ; (f) volumetric energy dissipation versus d/a ratio for member ductility of $\mu = 10$

Fig. 7. Variation of BRB elastic axial forces ratio with bridge geometric relations and skew angle (φ) (for EDS-2); (a) for $P_L/P_T = 0.30$ and $s/a = 0.50$; (b) for $P_L/P_T = 0.40$ and $s/a = 0.50$; (c) for $P_L/P_T = 0.30$ and $s/a = 1.00$; (d) for $P_L/P_T = 0.40$ and $s/a = 1.00$
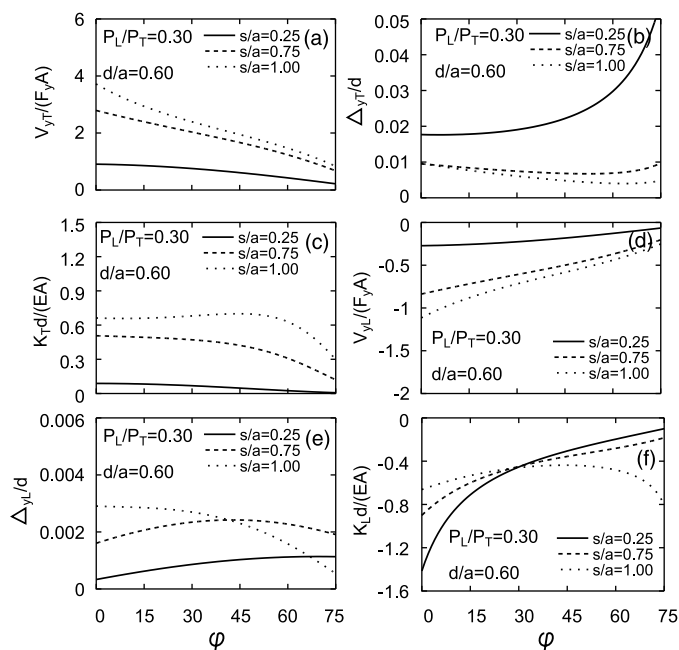
Fig. 8. Variation of behavioral characteristics when short BRBs yield: (a) nondimensional transverse base shear strength versus skew angle φ; (b) transverse yield drift versus φ; (c) nondimensional transverse stiffness versus φ; (d) nondimensional longitudinal base shear strength versus φ; (e) nondimensional longitudinal yield drift versus φ; (f) nondimensional longitudinal stiffness versus φ

obtained in the transverse direction for small s/a ratios, both transverse and longitudinal drifts are much closer to each other, especially for larger φ angles. As shown in Fig. 8(f), longitudinal stiffness decreases as φ increases for the most practical values of s/a. For a wide range of skew angles, comparing transverse and longitudinal stiffnesses indicates that the stiffness in the longitudinal direction is larger than the transverse stiffness for smaller values of s/a. As φ and s/a increase, closer stiffnesses are obtained in both directions.

most ratios of s/a. Fig. 8(d) gives the variation of longitudinal base shear versus φ, revealing a decrease in this value with increasing skew angle. For smaller values of the s/a ratio, Fig. 8(e) illustrates an increase in the longitudinal drift (Δ_{yL}/d). This response is reversed for larger s/a ratios. Comparing transverse and longitudinal drift diagrams shows that although relatively larger drifts are
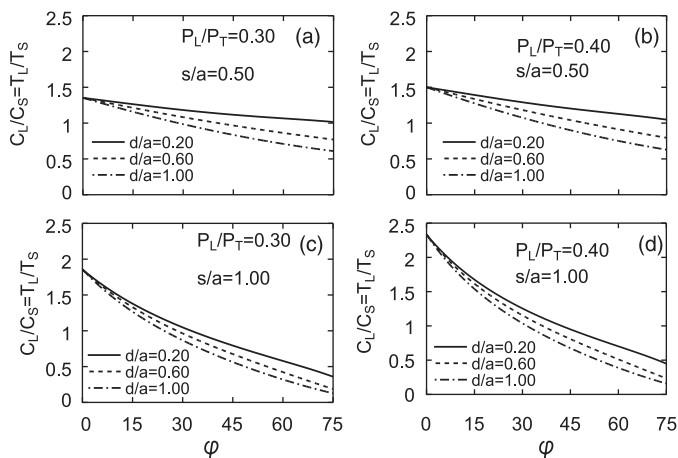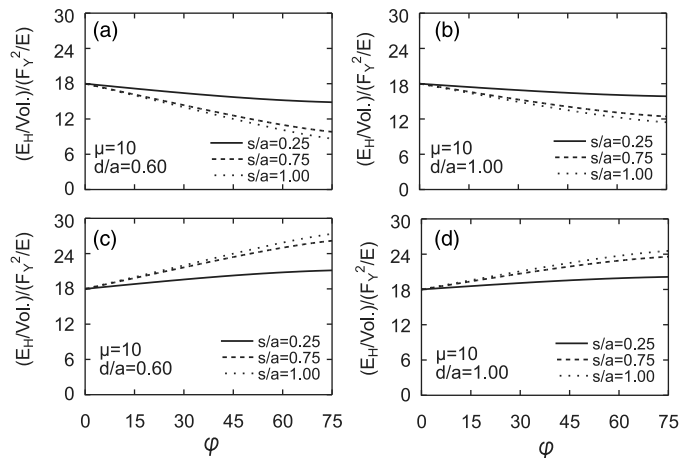

Fig. 9. Variation of volumetric energy dissipation with skew angle φ (for member ductility of $\mu = 10$): (a) short BRBs yield and $d/a = 0.60$; (b) short BRBs yield and $d/a = 1.00$; (c) long BRBs yield and $d/a = 0.60$; (d) long BRBs yield and $d/a = 1.00$

Hysteretic Energy Dissipation

The dissipated volumetric energy in this case can be given as follows:

$$\frac{E_H}{\text{Vol.}} = \frac{4(\mu - 1)\sqrt{1 + (s/a)^2 + (d/a)^2 - 2(s/a)\sin\varphi}}{\sqrt{1 + (s/a)^2 + (d/a)^2 - 2(s/a)\sin\varphi} + \sqrt{1 + (s/a)^2 + (d/a)^2 + 2(s/a)\sin\varphi}}\left(\frac{F_y^2}{E}\right) \tag{27}$$

Assuming $d/a = 0.60$, $\mu = 10$ and as depicted in Figs. 9(a) and 9(b), hysteretic energy decreases as φ increases. Changes in the s/a ratio have more effect on the dissipated energy at larger φ angles. Compared with $d/a = 0.60$, the end diaphragm system with $d/a = 1.00$ dissipates more energy at larger φ angles.

Inelastic Behavior When Long BRBs Yield

Long BRBs yield when $C_L/C_S = T_L/T_S > 1$. The inelastic behavior is governed by yielding of the long BRBs, and the system plastically displaces until the maximum displacement demand is reached, which is related to the member ductility demand. Again, an elastic-plastic inelastic behavior develops.

Response in the Transverse Direction

As was done for the previous case with short BRBs yielding to drive all relevant equations, but this time instead replacing the axial force values of long BRBs by their corresponding yield values, the following equations are obtained. The base shear is then equal to

$$V_{yT} = \left[\frac{4(s/a)\cos\varphi}{\sqrt{1 + (s/a)^2 + (d/a)^2 + 2(s/a)\sin\varphi}[(s/a)(P_L/P_T\cos\varphi - \sin\varphi) + 1]}\right](F_y A) \tag{28}$$

And, the transverse yield drift is

$$\begin{aligned}
\frac{\Delta_{yT}}{d} &= \{[1 + (s/a)^2 + (d/a)^2 + 2(s/a)\sin\varphi]^{3/2}[(s/a)\sin\varphi - 1][(s/a)(P_L/P_T\cos\varphi - \sin\varphi) + 1] \\
&+ [1 + (s/a)^2 + (d/a)^2 - 2(s/a)\sin\varphi]^{3/2}[(s/a)(P_L/P_T\cos\varphi - \sin\varphi) - 1][(s/a)\sin\varphi + 1]\} \\
&\times \left(\frac{F_y}{E}\right)/2(d/a)(s/a)\sqrt{1 + (s/a)^2 + (d/a)^2 + 2(s/a)\sin\varphi}\cos\varphi[(s/a)(-P_L/P_T\cos\varphi + \sin\varphi) - 1]
\end{aligned} \tag{29}$$

As expected, the initial stiffness of the system in the transverse direction is the same as that for the short BRBs yielding case.

Response in the Longitudinal Direction

Performing equilibrium equations in the longitudinal direction gives the longitudinal base shear at long BRBs yielding as

$$V_{yL} = \left[\frac{4(s/a)(P_L/P_T)\cos\varphi}{\sqrt{1 + (s/a)^2 + (d/a)^2 + 2(s/a)\sin\varphi}[(s/a)(\sin\varphi - P_L/P_T\cos\varphi) - 1]}\right](F_y A) \tag{30}$$

The following formula is obtained for the yield drift in the longitudinal direction:

$$\begin{aligned}
\frac{\Delta_{yL}}{d} &= \{[1 + (s/a)^2 + (d/a)^2 + 2(s/a)\sin\varphi]^{3/2}[(s/a)(P_L/P_T\cos\varphi - \sin\varphi) + 1] \\
&+ [1 + (s/a)^2 + (d/a)^2 - 2(s/a)\sin\varphi]^{3/2}[(s/a)(P_L/P_T\cos\varphi - \sin\varphi) - 1]\} \\
&\times \left(\frac{F_y}{E}\right)/2(d/a)\sqrt{1 + (s/a)^2 + (d/a)^2 + 2(s/a)\sin\varphi}[(s/a)(P_L/P_T\cos\varphi - \sin\varphi) + 1]
\end{aligned} \tag{31}$$

Again, the initial stiffness of the system in the transverse and longitudinal directions can be produced using Eqs. (28), (29), (31), and (32). Since the general behavioral tendency is similar to those for the short BRBs yielding case, no further figures are presented. The initial stiffness of the system in the longitudinal direction is the same as for the case of short BRBs yielding.

Hysteretic Energy Dissipation

In case of longitudinal BRBs yielding, this value is obtained as

$$\frac{E_H}{\text{Vol.}} = \frac{4(\mu - 1)\sqrt{1 + (s/a)^2 + (d/a)^2 + 2(s/a)\sin\varphi}}{\sqrt{1 + (s/a)^2 + (d/a)^2 - 2(s/a)\sin\varphi} + \sqrt{1 + (s/a)^2 + (d/a)^2 + 2(s/a)\sin\varphi}}\left(\frac{F_y^2}{E}\right) \tag{32}$$

Again, assuming $d/a = 0.60$ and $\mu = 10$, Figs. 9(c) and 9(d) show that the dissipated energy increases as the skew angle increases because larger φ angles result in longer BRBs that also leads to high volume of long BRBs and thus larger dissipated energy. Compared with $d/a = 0.60$, the retrofit system with $d/a = 1.00$ dissipates less energy at larger skew angles.

Special Cases

Although the previously derived general equations for EDS-1 and EDS-2 are complex, because of the large number of geometric parameters that they consider, they take simpler forms in special cases. For example, for nonskewed bridges ($\varphi = 0°$), simpler

formulas are obtained by substituting $\varphi = 0$ in the relevant equations and are given in detail in Celik and Bruneau (2007). Additionally, the impact of several loading ratios on the inelastic behavior of skewed systems is numerically investigated in Celik and Bruneau (2007).

Numerical Example

Two ductile end diaphragm systems, namely, S1 and S2, are selected (Fig. 10). Comparison between S1 and S2 is important to assess the relative effectiveness of the end diaphragm configurations on the inelastic behavior for skewed systems. Special emphasis is placed on hysteretic energy dissipation. S1 and S2 are highly skewed systems ($\varphi = 45°$) having BRB configurations that correspond to EDS-1 and EDS-2, respectively. In S2, because of the presence of skewness, the lengths of the BRBs are not equal to each other and thus "short" and "long" BRBs exist. Comparison between skewed systems such as S1 and S2 and nonskewed systems similar to S1 and S2 is also worthwhile and given in Celik and Bruneau (2007).

The geometrical dimensions of these systems are arbitrarily selected in simplicity and are not intended to correspond to a specific bridge. For this purpose, a system having a side length of 914.4 mm (36″) is selected for the analyses. Both unidirectional and bidirectional loadings are considered to show the effect of bidirectional earthquake effects. It is assumed that the BRBs have a target displacement ductility of $\mu = 4$, a yield point of $F_y = 345$ MPa (50 ksi), and a modulus of elasticity of $E = 200,000$ MPa (29,000 ksi). No effort has been made to calculate actual ductility demands in the BRBs; instead, for comparison purposes and for simplicity, a displacement ductility of $\mu = 4$ is assumed in this example. Higher values can be established through more rigorous pushover analysis for a bridge under consideration. Other system properties are summarized in Table 1.

Static unidirectional (in X or Y directions) and bidirectional (labeled $X + Y$) pushover analyses are conducted using SAP2000. Note that X and Y indicate the transverse (T) and longitudinal (L) directions, respectively. Using SAP2000 results and the formulas developed in this paper, the system parameters and responses of each system are summarized in Table 1.

To compare the effectiveness of each system, similar systems are defined as having either BRBs with same cross-sectional area (SA), BRBs with the same base shear strength (SBS) in the governing direction, and BRBs with the same initial stiffness (SIS). For each case, results are typically presented for the base shear at yield (V_B) in the governing direction, the initial stiffness in the governing direction (K_E), the corresponding yield displacement (Δ_y),

the maximum displacement reached (Δ_{max}), hysteretic energy dissipated (E_H) at $\mu = 4$, the volumetric energy dissipation (E_H/Vol.), which is the energy dissipated per BRB material used, and the effectiveness ratio (with respect to an arbitrarily chosen reference system having similar properties) to each system in terms of hysteretic energy dissipation. Note that E_H is calculated by using the area under $1/4$ of a complete hysteretic loop. The following observations can be made from Table 1:

- Under loading in the X direction and for SA, compared with S2, S1 has greater base shear strength, yield, and maximum displacement demands as well as total and volumetric hysteretic energies, but lower initial stiffness. S1 used 68% more bracing material. For SBS in the transverse direction, compared with S2, S1 has greater yield and maximum displacements and total and volumetric hysteretic energy dissipations but lower initial stiffness and required cross-sectional area. S1 used 11% more material. For SIS, all structural response characteristics are greater in S1 than in S2. In all cases, under the effect of transverse loading, the effectiveness ratios for S1 and S2 are 1.00 and 0.75, respectively.

- Under unidirectional loading in the longitudinal (Y) direction and for SA, compared with S2, S1 has greater base shear capacity, initial stiffness, and total hysteretic energy dissipation but lower yield and maximum displacements, and volumetric hysteretic energy dissipation. In this case, 68% more BRB material is used in S1. For SBS compared with S2, S1 has greater initial stiffness but lower yield and maximum displacement demands, required cross-sectional area, and total and volumetric hysteretic energy dissipations. S1 used 13% more material. For SIS in the longitudinal direction, all structural response characteristics are lower in S1 than in S2. S2 also used 19% more BRB material. In all cases, under the effect of longitudinal loading, the effectiveness ratios for S1 and S2 are 0.80 and 1.00, respectively. The efficiency is reversed under the longitudinal and bidirectional loadings compared with transverse loading, since the yielding BRBs change in S2. When long BRBs yield in S2, the system dissipates more energy as compared with S1.

- Under two-directional loading, investigating the systems' response in each of the principal orthogonal directions is appropriate. For SA and considering the transverse response in the transverse direction under bidirectional loading, compared with S2, S1 has greater base shear capacity, initial stiffness, and yield and maximum displacement demands. Since the axial forces of the BRBs in the longitudinal direction are zero, S1 does not displace and no energy is dissipated for this particular case, i.e., for the selected bridge geometry and bidirectional loading ratio.
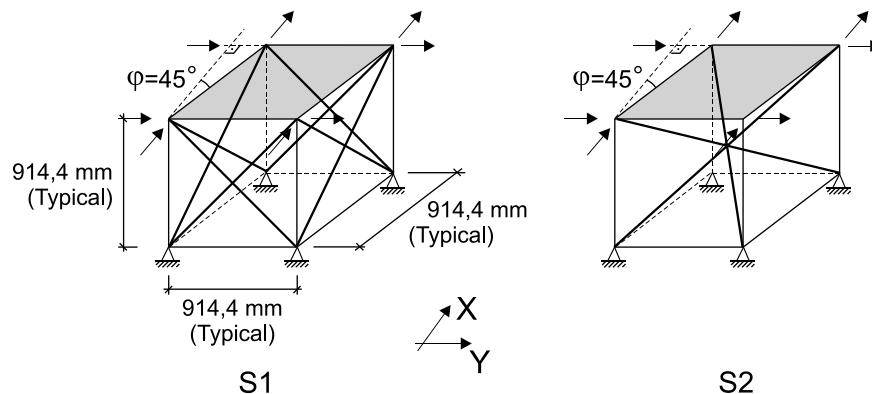

Fig. 10. Selected skewed systems representing various end diaphragm BRB configurations (for Table 1)

Table 1. Effect of Bracing Configuration on Hysteretic Energy Dissipation for Skewed Bridges ($\varphi = 45°$)

System	Info		V_B (kN)	K_E (kN/mm)	Δ_y (mm)	Δ_{max} (mm)	μ_G	A (mm²)	L_L (mm)	L_S (mm)	LOAD	E_H (kN.mm)	Vol. (mm³)	E_H/Vol (10^{-3}) (kN mm/mm³)	Eff. Ratio
S1	SA	T	444.85	66.50	6.69	20.12	3.01	645.16	1293.11	NA	X	5974.34	6674103	0.89	1.00
S2	SA	T	292.65	85.32	3.43	12.51	3.65	645.16	1921.26	1151.38	X	2657.26	3964689	0.67	0.75
S1	SBS	T	125.81	18.81	6.69	20.12	3.01	182.45	1293.11	NA	X	1689.62	1887423	0.89	1.00
S2	SBS	T	125.81	36.68	3.43	12.51	3.65	277.42	1921.26	1151.38	X	1142.35	1704824	0.67	0.75
S1	SIS	T	444.85	66.50	6.69	20.12	3.01	645.16	1293.11	NA	X	5974.34	6674103	0.89	1.00
S2	SIS	T	228.28	66.50	3.43	12.51	3.65	503.22	1921.26	1151.38	X	2072.78	3092428	0.67	0.75
S1	SA	L	629.11	199.7	3.15	12.60	4.00	645.16	1293.11	NA	Y	5945.09	6674103	0.89	0.80
S2	SA	L	423.47	100.1	4.23	14.70	3.48	645.16	1921.26	1151.38	Y	4434.65	3964689	1.12	1.00
S1	SBS	L	177.93	56.5	3.15	12.60	4.00	182.45	1293.11	NA	Y	1683.47	1887423	0.89	0.80
S2	SBS	L	177.93	42.1	4.23	14.70	3.48	271.10	1921.26	1151.38	Y	1863.12	1665985	1.12	1.00
S1	SIS	L	629.11	199.7	3.15	12.60	4.00	645.16	1293.11	NA	Y	5945.09	6674103	0.89	0.80
S2	SIS	L	847.48	199.7	4.23	14.70	3.48	1291.22	1921.26	1151.38	Y	8874.96	7934908	1.12	1.00
S1	SA	T	444.85	99.7	4.46	17.88	4.00	645.16	1293.11	NA	X + Y	5969.89	6674103	0.89	0.80
		L	444.85	—	0	0	NA								
S2	SA	T	299.41	92.1	3.25	7.59	2.34	645.16	1921.26	1151.38	X + Y	4434.26	3964689	1.12	1.00
		L	299.41	109.7	2.73	13.20	4.84								
S1	SBS	T	125.81	28.2	4.46	17.88	4.00	182.50	1293.11	NA	X + Y	1688.24	1887941	0.89	0.80
		L	125.81	—	0	0	NA								
S2	SBS	T	125.81	38.7	3.25	7.59	2.34	271.10	1921.26	1151.38	X + Y	1863.10	1665962	1.12	1.00
		L	125.81	46.1	2.73	13.20	4.84								

The BRBs in the skew direction yield in this case (four out of eight). The overall behavior is bidirectional in S2, i.e., it displaces in both orthogonal directions; and after the yielding of long BRBs, the system moves significantly in the longitudinal direction and reaches its maximum displacement. From Table 1, the numeric values of the global displacement ductilities (μ_G) in both transverse and longitudinal directions are calculated as 2.34 and 4.84, respectively, keeping in mind that the BRBs used a member (local) displacement ductility of 4. As compared with S2, S1 has greater longitudinal base shear strength and total hysteretic energy dissipation but lower energy dissipated per BRB volume. S1 used 68% more bracing material. For SBS in the transverse direction, compared with S2, S1 has greater yield and maximum displacements but lower initial stiffness. Again, no response is obtained in the longitudinal direction in S1, as explained previously. The behavior is also bidirectional in S2 and after the yielding of long BRBs, the system displaces in the longitudinal direction significantly; the global ductilities are the same as above. Compared with S2, S1 has lower required cross-sectional area, total and volumetric hysteretic energy dissipations, and 13% more material is used in S1, eight braces in S1, four braces in S2. In all cases, effectiveness ratios for S1 and S2 are 0.80 and 1.00, respectively. Lower required cross-sectional areas for the BRBs lead to lower axial yield forces and thus create lower-end connection forces that could be desirable in seismic design.

Conclusions

Numerical pushover analyses have been conducted on two ductile end diaphragms configurations, EDS-1 and EDS-2, incorporating BRBs and developed to provide seismic resistance of skewed steel bridges under bidirectional earthquake excitation. Results indicate that:

1. Skewness has a more severe impact on the end diaphragms' seismic behavior, although not a significant one until $\varphi \geq 30°$. Although the base shear strength and lateral stiffness decrease as the skew angle increases, drifts increase instead.

2. For EDS-1, smaller drifts are obtained in skewed bridges for larger d/a values and do not change much after $d/a = 1.00$. Also, dissipated energy per BRB volume used is less affected after $d/s = 1.00$. These results suggest that appropriate values for both d/a and d/s ratios could be selected between 0.5 and 1.0. A similar observation is made for EDS-2, as larger s/a ratios have a lesser impact on the behavioral characteristics, e.g., base shear, drift, and stiffness, as well as the dissipated energy. Appropriate values for the s/a ratio could also be selected between 0.5 and 1.0. Severely skewed systems had a poorer response and should be avoided if possible.

3. Under bidirectional loading and for a given required design base shear, compared with S2, S1 achieves lower required cross-sectional area and total and volumetric hysteretic energy dissipations. The EDS-1 configuration therefore seems to be more effective. Lower required cross-sectional areas for the BRBs lead to lower axial forces and smaller BRBs, and thus create lower end connection forces, resulting in simpler connections to superstructure and substructure that could be desirable in seismic design. However, S1 has the advantage over S2 to result in a more flexible ductile diaphragm. Flexible ductile end diaphragms can be desirable in bridges with relatively flexible substructures in which the end diaphragms need to reach a larger lateral displacement for a given member ductility.

4. Some of the assumptions made in this paper could be eliminated in future analytical work. For example, diaphragms having BRBs of unequal area, if deemed to be useful in some applications, could be investigated. "Tuning" the BRB areas to have yielding in both orthogonal directions at the same time might provide an efficient design and better seismic response in some cases, but not necessarily so, considering that the bridge is skewed and that the earthquake excitation is bidirectional with an unpredictable orientation of strongest ground motions.

Acknowledgments

References

AASHTO. (2002). *Standard specifications for highway bridges*, Washington, DC.

AASHTO. (2009). *Guide specifications for LRFD seismic bridge design*, 17th Ed., Washington, DC, 248.

ATC-32. (1996). *Improved seismic design criteria for California bridges: Provisional recommendations*, California-Washington, DC.

Black, C., Makris, N., and Aiken, I. (2002). "Component testing, stability analysis and characterization of buckling-restrained unbonded braces." *PEER Rep., 2002/08*, Pacific Earthquake Engineering Research Center, University of California, Berkeley.

Bruneau, M., Wilson, J. C., and Tremblay, R. (1996). "Performance of steel bridges during the 1995 Hyogo-ken Nanbu (Kobe, Japan) earthquake." *Can. J. Civil Eng.*, 23(3), 678–713.

Carden, L. P., Itani, A. M., and Buckle, I. G. (2006). "Seismic performance of steel girder bridges with ductile cross-frames using buckling-restrained braces." *J. Struct. Eng.*, 132(3), 338–345.

Celik, O. C., and Bruneau, M. (2007). "Seismic behavior of bidirectional-resistant ductile end diaphragms with unbonded braces in straight or skewed steel bridges." *Technical Rep. MCEER-07-0003*, MCEER, Buffalo, NY.

Computers and Structures, Inc. (CSI). (1998). *SAP2000 Integrated finite element analysis and design of structures—detailed tutorial including pushover analysis*, Berkeley, CA.

Itani, A. M., Bruneau, M., Carden, L., and Buckle, I. G. (2004). "Seismic behavior of steel girder bridge superstructures." *J. Bridge Eng.*, 9(3), 243–249.

Kanaji, H., Kitazawa, M., and Suzuki, N. (2003). "Seismic retrofit strategy using damage control design concept and the response reduction effect for a long-span truss bridge." *19th US-Japan Bridge Eng. Workshop-Panel on Wind and Seismic Effects*, US–Japan Cooperative Program in Natural Resources, Tsukuba Science City, Japan.

Lopez, W., and Sabelli, R. (2004). "Seismic design of buckling-restrained braced frames." *Steel Tips*, Structural Steel Educational Council, Moraga, CA, 78.

MCEER/ATC. (2003). "Recommended LRFD guidelines for the seismic design of highway bridges (MCEER/ATC-49)—Part I: Specifications and Part II: Commentary and Appendices," *Rep. MCEER-03-SP03*, MCEER/ATC Joint Venture, Buffalo, NY.

Sabelli, R., Mahin, S., and Chang, C. (2003). "Seismic demands on steel braced frame buildings with buckling-restrained braces." *Eng. Struct.*, 25(5), 655–666.

Sarraf, M., and Bruneau, M. (1998a). "Ductile seismic retrofit of steel deck-truss bridges. I: Strategy and modeling." *J. Struct. Eng.*, 124(11), 1253–1262.

Sarraf, M., and Bruneau, M. (1998b). "Ductile seismic retrofit of steel deck-truss bridges. II: Design applications." *J. Struct. Eng.*, 124(11), 1263–1271.

Zahrai, S. M., and Bruneau, M. (1998). "Impact of diaphragms on seismic response of straight slab-on-girder steel bridges." *J. Struct. Eng.*, 124(8), 938–947.

Zahrai, S. M., and Bruneau, M. (1999a). "Ductile end-diaphragms for seismic retrofit of slab-on-girder steel bridges." *J. Struct. Eng.*, 125(1), 71–80.

Zahrai, S. M., and Bruneau, M. (1999b). "Cyclic testing of ductile end-diaphragms for slab-on-girder steel bridges." *J. Struct. Eng.*, 125(9), 987–996.